Supplementary Materials

A luminescent sensor based on Zn(II) coordination polymer behave selective and sensitive detection for NACs and Fe^{3+} ions

Xiao zhang*, Xinrui Zhuang, Nanxi Zhang, Chunyu Ge, Xuan Luo, Jinxue Li, Jie Wu*, Qingfeng Yang, Rui Liu

Caption of Figures

Fig. S1 A view of the asymmetric unit and some symmetry-related atoms in **1**.

Fig. S2 Disordered TBA^{2-} anions in **1**. (a) component 1, (b) component 2, (c) both components.

Fig. S3 Powder XRD of simulated from the single-crystal data of **1** (black) and synthesized compound **1** (red)**.**

Fig. S4 Thermogravimetric analyses curve of **1**, the weight loss of 77.6 % is close to the calculated value (78.3 %).

Fig. S5 Powder XRD of ZnO from the combustion residue and reference card of ZnO.

Fig. S6 The IR spectra of H_2TBA ligand and **1**.

Fig. S7 Solid - state emission spectra of compound **1** and free H_2TBA and 4,4-bipy ligand when excited at 285 nm, 276 nm, 362 nm, respectively.

Fig. S8 Emission spectra of **1** dispersed in different solvents when excited at 290 nm.

Fig. S9 Power XRD patterns of **1** immersed in different solvents at room temperature.

Fig. S10 (a) The luminescence intensity of **1** upon incremental addition of PA solution (5 mM) in water. (b) Stern-Volmer plot for the luminescence intensity of **1** upon the addition of PA solution (5 mM) in water.

Fig. S11 The luminescence intensity of **1** upon incremental addition of NACs solution (5 mM) in water (a: NB, b: 4-Np, c: 2,4-DNT, d: m-NT, e: m-DNB, f: p-NT, g: o-NT).

Fig. S12 The fitting curve of the luminescence intensity of **1** at different PA concentration.

Fig. S13 HOMO and LUMO of ligand and NACs

Fig. S14. Spectral overlap between absorbance spectra of NACs and emission spectra of **1**.

Fig. S15 The fitting curve of the luminescence intensity of **1** at different Fe^{3+} concentration

Fig. S16 Powder XRD patterns of simulated from the single-crystal data of **1** and synthesized compound and Fe^{3+}-**1.**

Fig. S17 IR spectra of compound **1** and **1**/Fe^{3+}.

Fig. S18 The XPS of Fe^{3+}-**1** shows the typical peak of Fe^{3+} at 710 Ev

Fig. S19 Spectral overlap between absorbance spectra of metal icons and emission spectra of **1**

Caption of Tables

Table S1 Selected bond lengths (Å) and angles (°) for **1**

Table S2 Summary of quenching constants (K_{SV}) for **1** sensing of NACs at room temperature.

Table S3 HOMO and LUMO energies for calculated NACs and ligand at B3LYP/6-31G* level of theory.

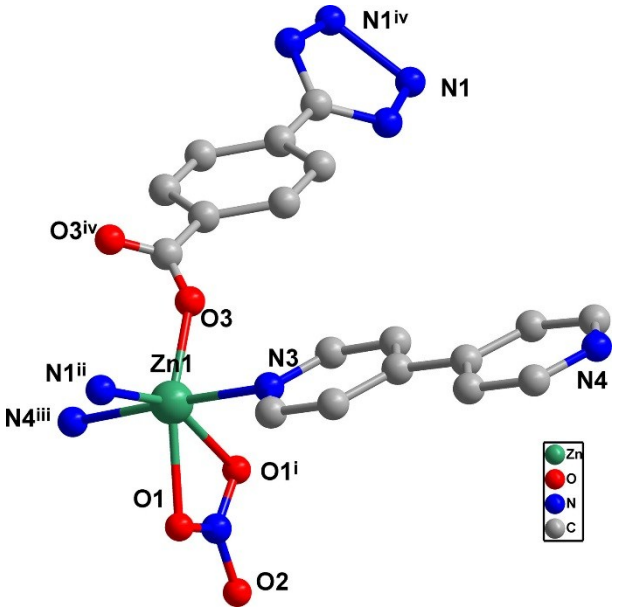

Fig. S1 A view of the asymmetric unit and some symmetry-related atoms in **1**. (Symmetry codes: (i) x, -y, z, 2-z; (ii) x, 1+y, z; (iii) -1+x, y, z; (iv) –x, y).

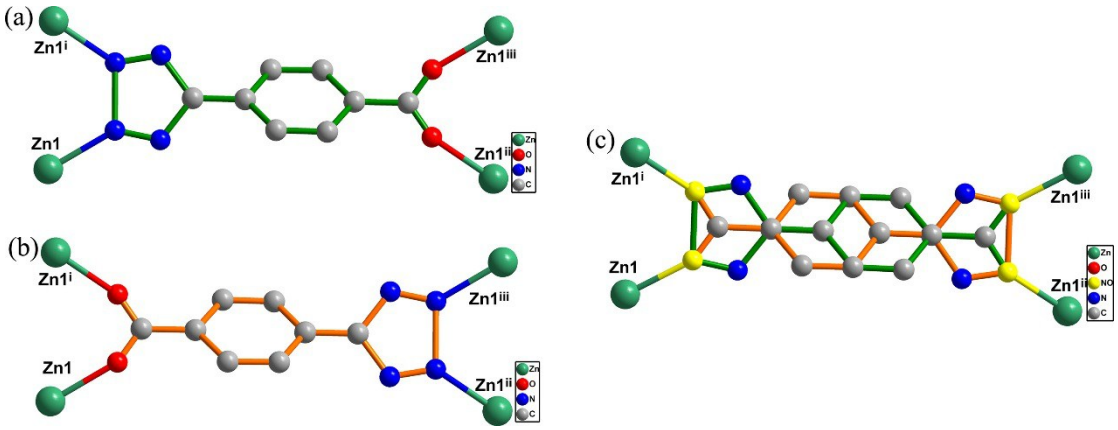

Fig. S2 Disordered TBA^{2-} anions in **1**. (a) component 1, (b) component 2, (c) both components

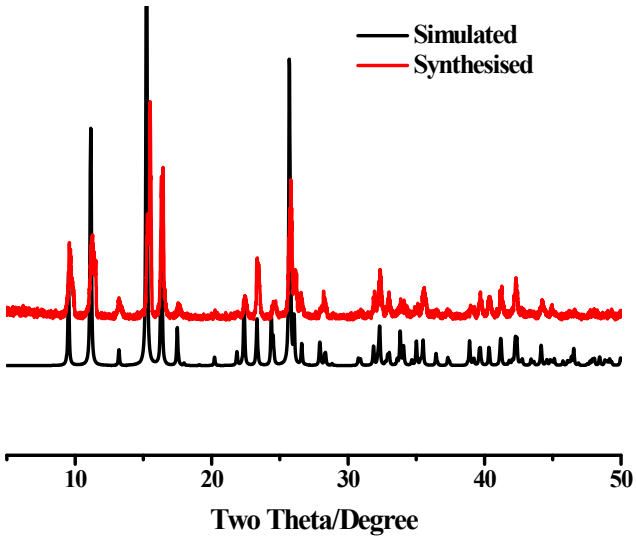

Fig. S3 Powder XRD of simulated from the single-crystal data of **1** (black) and synthesized compound **1** (red)**.**

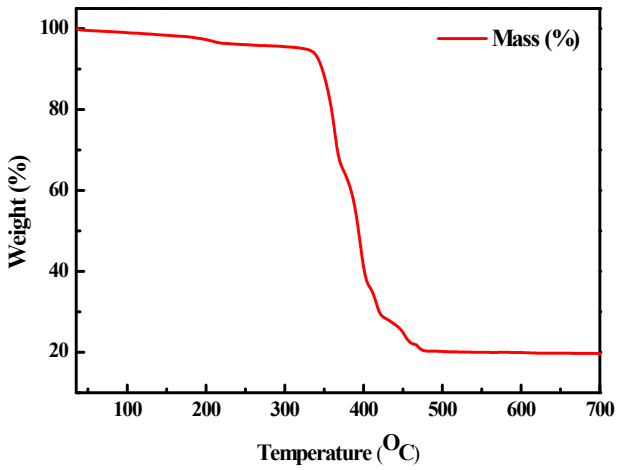

Fig. S4 Thermogravimetric analyses curve of **1**, the weight loss of 77.6 % is close to the calculated value (78.3 %).

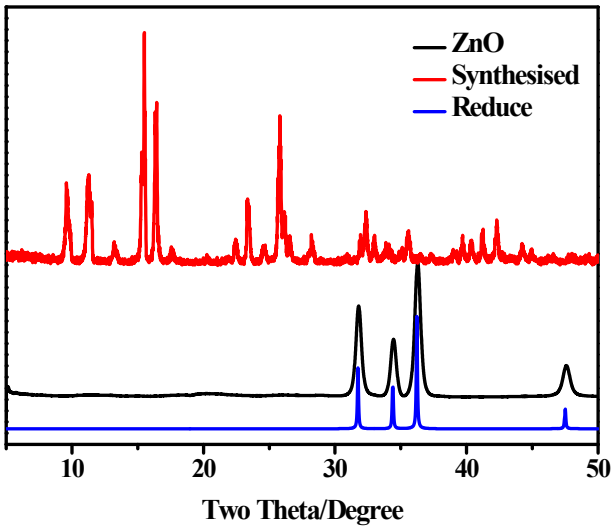

Fig. S5 Powder XRD of ZnO from the combustion residue and reference card of ZnO.

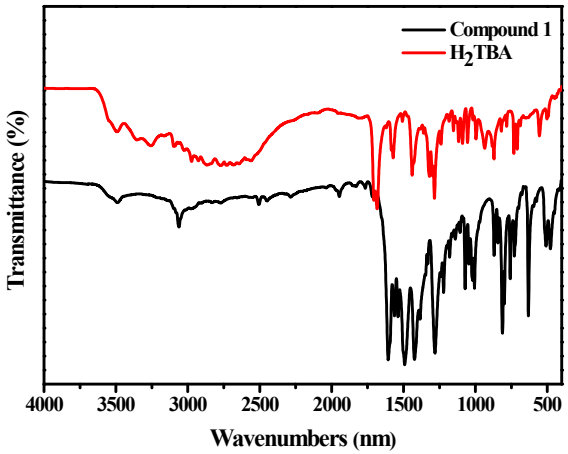

Fig. S6 The IR spectra of H_2TBA ligand and **1**.

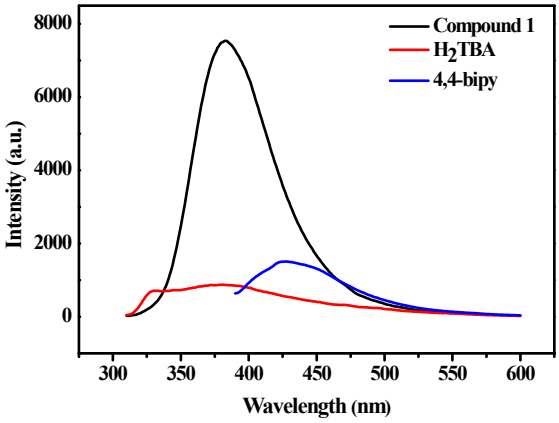

Fig. S7 Solid-state emission spectra of compound **1,** free H_2TBA and 4,4'-bipy ligand when excited at 285 nm, 276 nm, 362nm, respectively.

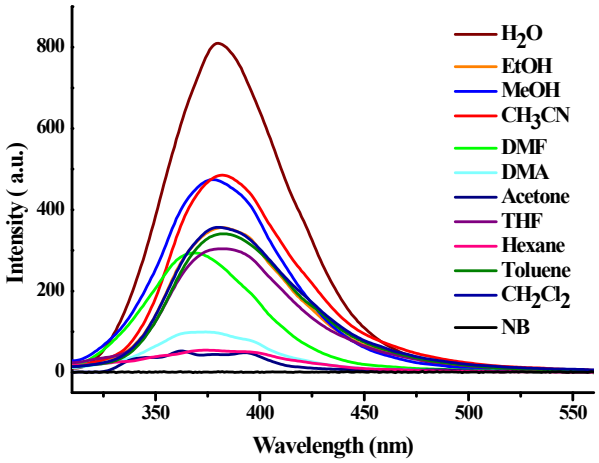

Fig. S8 Emission spectra of **1** dispersed in different solvents when excited at 290 nm.

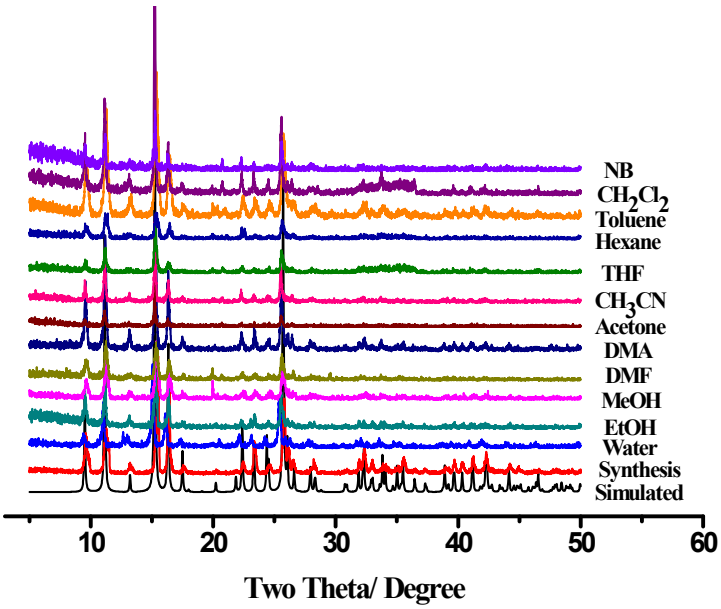

Fig. S9 Power XRD patterns of **1** immersed in different solvents at room temperature.

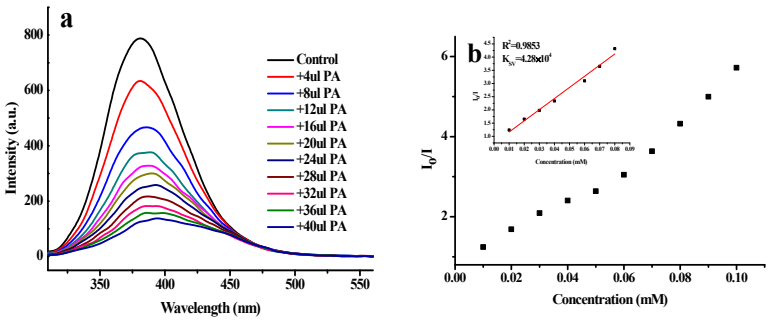

Fig. S10 (a) The luminescence intensity of **1** upon incremental addition of PA solution (5 mM) in water. (b) Stern-Volmer plot for the luminescence intensity of **1** upon the addition of PA solution (5 mM) in water.

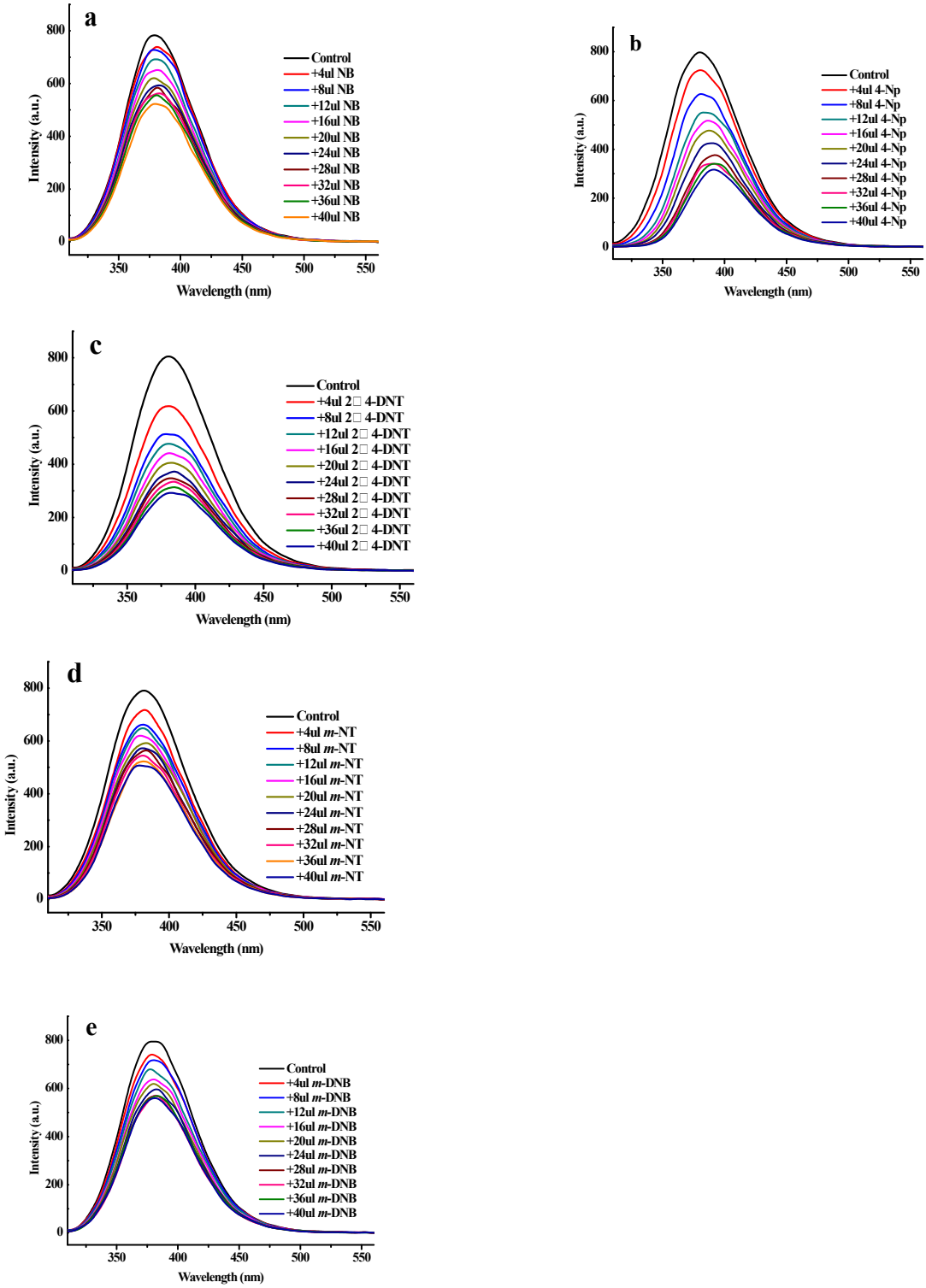

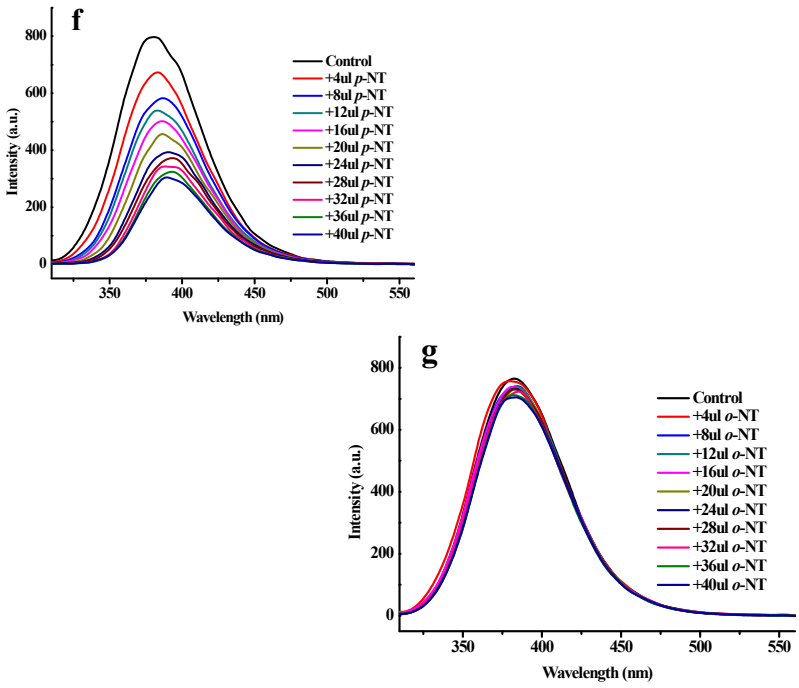

Fig. S11 The luminescence intensity of **1** upon incremental addition of NACs solution (5 mM) in water (a: NB, b: 4-Np, c: 2,4-DNT, d: m-NT, e: m-DNB, f: p-NT, g: o-NT)

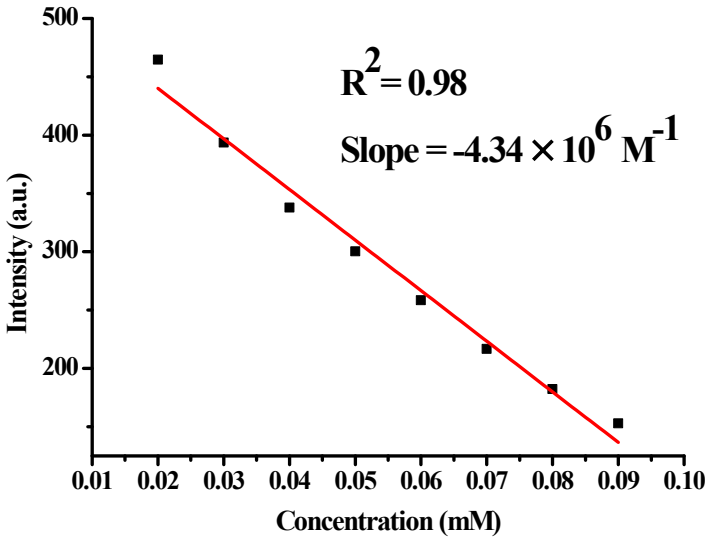

Slope = - 4.34 × 10^6 M^{-1}

δ = 8.72 (N = 10)

Limit detection = 3δ/Slope = 6.02 × 10^{-6} M

Fig. S12 The fitting curve of the luminescence intensity of **1** at different PA concentration .

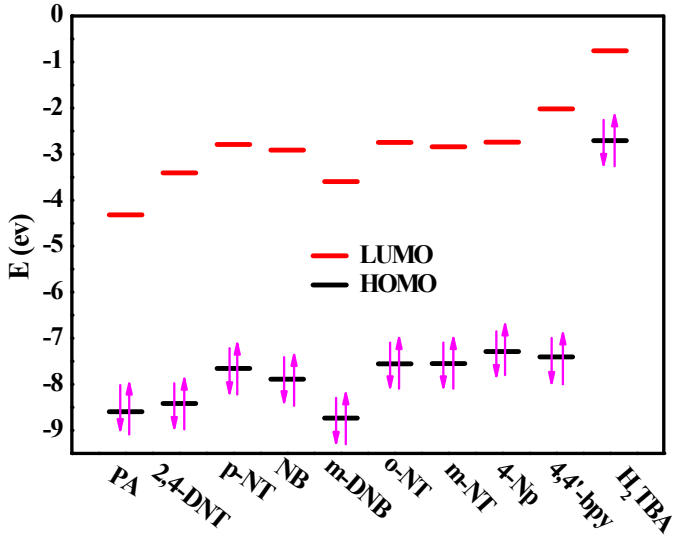

Fig. S13 HOMO and LUMO of ligand and NACs.

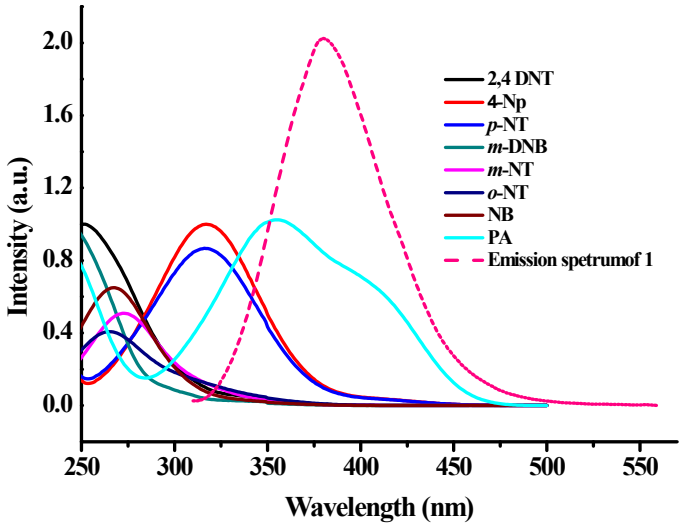

Fig. S14 Spectral overlap between normalized absorbance spectra of NACs and emission spectra of **1**.

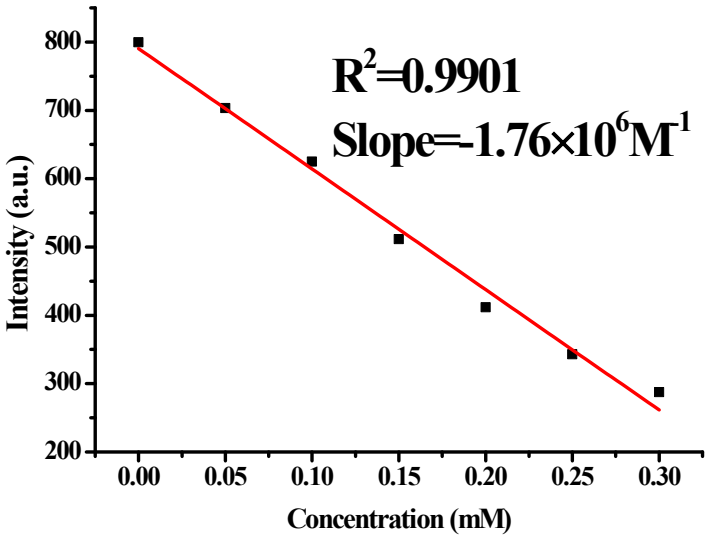

Linear Equation: Y = -1763.85X + 790.53

R = 0.9901

Slope = 1.76×10^{6} M^{-1}

δ=4.21 (N=10)

Limit detection =3δ/Slope=7.18×10^{-6} M

Fig. S15 The fitting curve of the luminescence intensity of **1** at different Fe^{3+} concentration.

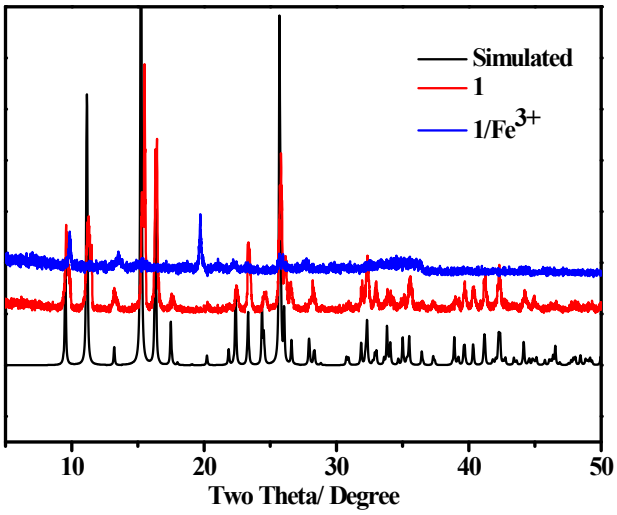

Fig. S16 Powder XRD patterns of simulated from the single-crystal data of **1** and synthesized compound and Fe^{3+}-**1**.

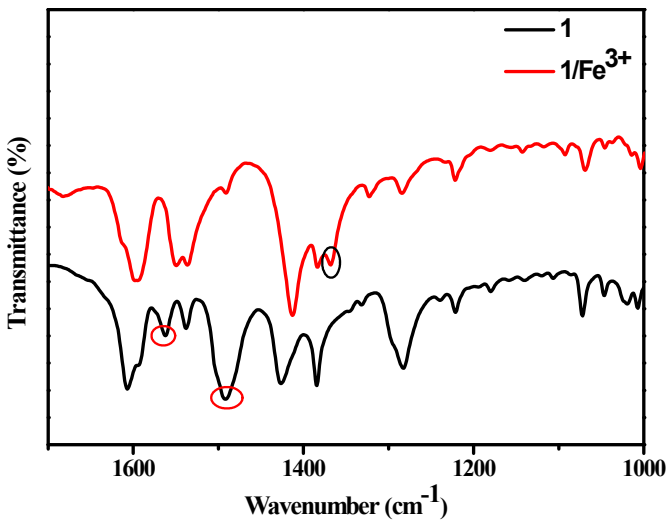

Fig. S17 IR spectra of compound **1** and **1**/Fe^{3+}.

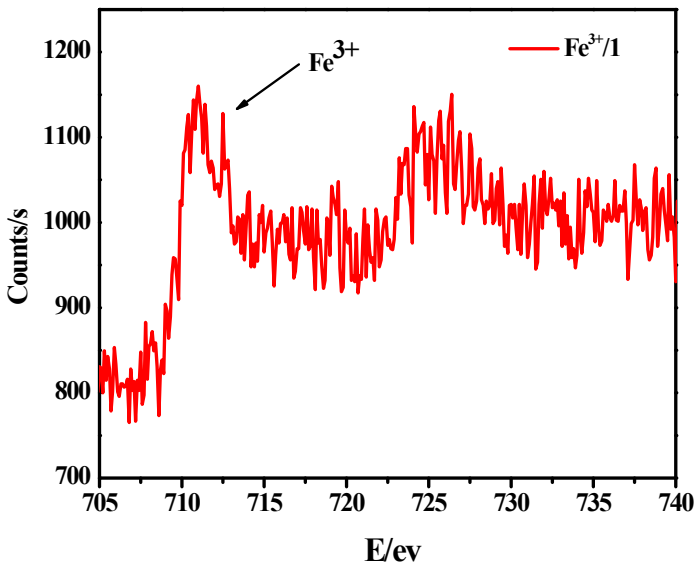

Fig. S18 The XPS of Fe^{3+}-**1** shows the typical peak of Fe^{3+} at 710 Ev.

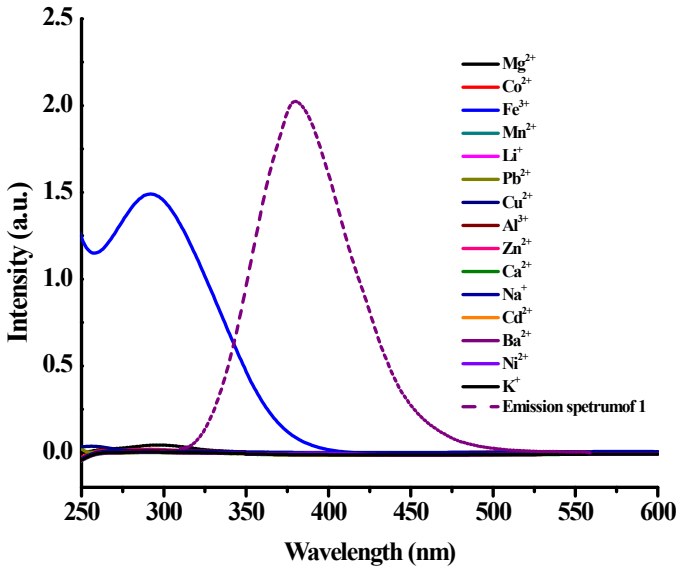

Fig. S19 Spectral overlap between absorbance spectra of metal icons and emission spectra of **1**.

Table S1 Selected bond lengths (Å) and angles (o) for **1**.

Zn1-O1	2.202(6)	Zn1-N5	2.522(10)
O1-Zn1-N4^{2}	86.2(2)	O1^{1}-Zn1-N5	29.31(18)
N1-Zn1-O1	153.6(3)	N1-Zn1-N1^{1}	110.9(4)
N1^{1}-Zn1-N3	91.6(2)	N1^{1}-Zn1-N4^{2}	89.56(19)
O3^{1}-Zn1-O1^{1}	153.6(3)	N4^{2}-Zn1-N5	84.3(3)

Symmetry codes ^{1}+X,-Y,+Z; ^{2}-1+X,+Y,+Z; ^{3}-X,+Y,2-Z; ^{4}+X,1-Y,+Z; ^{5}1+X,+Y,+Z; ^{6}-X,1-Y,2-Z

Table S2 Summary of quenching constants (K_{SV}) for **1** sensing of NACs at room temperature.

Nitro explosives	K_{SV} (M^{-1})
PA	4.83×10^{4}
NB	4.94×10^{3}
m-DNB	5.5×10^{3}
o-NT	7.68×10^{3}
m-NT	5.00×10^{3}
p-NT	1.61×10^{4}
2,4-DNT	1.49×10^{4}
4-Np	1.62×10^{4}

Table S3 HOMO and LUMO energies for calculated NACs, H_2TBA and 4,4'-bpy at B3LYP/6-31G* level of theory.

Analytes	HOMO (ev)	LUMO (ev)	Bond gap
PA	-8.595166	-4.320934	4.27432
2,4-DNT	-8.41361	-3.409107	5.004502
p-NT	-7.655022	-2.79225	4.862798
NB	-7.887787	-2.912631	4.975156
m-DNB	-8.730522	-3.596104	5.134419
o-NT	-7.554773	-2.746777	4.807996
m-NT	-7.55031	-2.838932	4.711378
4-Np	-7.290064	-2.73967	4.550394
4,4’-bpy	-7.402589	-2.01690	5.273164
H2TBA	-2.7089546	-0.75771814	1.95123646